

Trade-offs between structural richness and communication efficiency in music network representations

Lluc Bono Rosselló,^{1,*} Robert Jankowski,^{2,3,4} Hugues Bersini,¹ Marián Boguñá,^{3,4} and M. Ángeles Serrano^{3,4,5}

¹*Institute for Interdisciplinary Studies on Artificial Intelligence (IRIDIA),
Université Libre de Bruxelles, Brussels, Belgium*

²*Faculty of Electrical Engineering, Mathematics and Computer Science,
Delft University of Technology, 2628 CD, Delft, Netherlands*

³*Departament de Física de la Matèria Condensada,
Universitat de Barcelona, Martí i Franquès 1, E-08028 Barcelona, Spain*

⁴*Universitat de Barcelona Institute of Complex Systems (UBICS), Universitat de Barcelona, Barcelona, Spain*

⁵*ICREA, Passeig Lluís Companys 23, E-08010 Barcelona, Spain*

(Dated: March 12, 2026)

Music is a structured and perceptually rich sequence of sounds in time, whose perception is shaped by the interplay of expectation and uncertainty about what comes next. Yet the uncertainty we infer from music depends on how the musical piece is encoded as an event sequence. In this work, we use network representations, in which event types are nodes and observed transitions are directed edges, to compare how different feature encodings shape the transition structure we recover and what this implies for both the descriptive uncertainty expectation under imperfect memory and noise. We systematically analyse eight encodings of piano music, from single-feature vocabularies to richer multi-feature combinations. These representational choices reorganize the state space and fundamentally reshape network topology, shifting how uncertainty is distributed across transitions. To connect these descriptive differences to perception, we adopt a perceptual-constraint model that captures imperfect access to transition statistics. Overall, compressed single-feature representations yield dense transition structures with higher entropy rates, corresponding to higher average uncertainty per step, yet low model error, indicating that the constrained estimate stays close to the corpus transitions. In contrast, richer multi-feature representations preserve finer distinctions but expand the state space, sharpen transition profiles, lower entropy rates, and increase model error. Finally, across representations, uncertainty concentrates in diffusion-central nodes while model error remains low there, suggesting an informational landscape in which predictable flow coexists with localized surprise. Overall, our results show that feature choice shapes not only the networks we reconstruct, but also whether their resulting uncertainty is a plausible proxy for the expectations listeners can realistically learn and use.

I. INTRODUCTION

Music is a highly complex phenomenon composed of low-level features that combine into patterns that incorporate multiple structural aspects. Gaining insight into how these patterns emerge from basic musical events offers a useful perspective for understanding both the complexity of music and the perceptual processes involved in listening [1, 2]. These perceptual processes include the formation of expectations about what comes next and the experience of varying uncertainty and surprise as those expectations are confirmed or violated [2–4].

Any analysis of musical structure depends on how the musical piece is encoded as a sequence of events. Musical sequences can be represented at different levels of detail by selecting subsets of features—such as pitch, interval, or duration—that preserve some distinctions while discarding others, an idea closely related to *viewpoint*-based approaches in music cognition [5]. These representational choices define the event vocabulary and its granularity, and therefore shape which regularities can be

expressed or detected, including uncertainty about what comes next. Accordingly, what matters is not only the overall level of this uncertainty, but also how it is organized in a piece [2, 3]. Since both depend on the chosen event vocabulary, representational choices can systematically reshape the uncertainty patterns we infer.

For example, consider a short melody of eight notes: (A4–C5–A5–F5–A6–C4–F4–A7). If we encode each note as a distinct event by combining pitch class and octave, the sequence contains eight different event types, so each event type tends to have only one observed next-event option, making transitions appear highly predictable. If, instead, we collapse octave and keep only pitch class, the same melody reduces to the pitch-class sequence (A–C–A–F–A–C–F–A) and to just three event types (A, C, and F) repeated across the eight notes. Each event type can then be followed by different events (e.g., A can be followed by either C or F), increasing uncertainty. Thus, although both encodings describe the same musical surface, they induce different transition statistics, raising a basic methodological question: how does representational detail shape the structure we infer from music?

One way to make such differences explicit is to use network representations, in which sequence elements are

* Corresponding author: Lluc.Bono.Rossello@ulb.be

modeled as nodes and observed transitions between elements as directed edges. Previous work used pitch-based representations with octave and duration [6, 7], pitch-class sets [8–12], and chord-split representations [13, 14], which resulted in different topologies and statistical insights [15–19]. Yet, without a systematic comparison across levels of detail within the same musical corpus, it remains unclear whether the reported topological patterns reflect the music itself or the encoding, motivating a cross-representation analysis that makes explicit how different event vocabularies redistribute uncertainty across the network.

Network representations allow us to describe how different encodings redistribute uncertainty. However, because expectation and surprise are perceptual phenomena, whether these descriptive uncertainties can serve as proxies for listeners’ expectations depends on how reliably the corresponding transition structure can be learned under imperfect memory and noise.

This raises a second question: under what conditions does a representation’s transition structure yield expectations that humans can realistically learn and use under perceptual constraints? Human responses to sequential input are limited by memory, noise, and representational cost [20–24]. A key consequence is that observers may not rely only on the immediately observed one-step transitions, but may partially integrate information over multiple steps—treating events that are reachable in two or more steps as if they were more directly available than the true statistics imply. Such integration can cause listeners to treat events that occur only after several steps as if they were possible next events, thereby changing the transition probabilities they infer. Recent work shows that communication efficiency under such perceptual constraints depends on the organization of uncertainty [20]. Lynn et al. [21] showed, using reaction-time experiments with visual sequences, that even when two sequences have the same average uncertainty, meaning that continuations are equally unpredictable, differences in the organization of transitions can cause humans to react as if the uncertainty were higher, resulting in a perceptual error, defined as the mismatch between the true transition statistics and the observer’s inferred model.

Returning to our melodic example, this suggests that the pitch-class+octave encoding should allow a single expected continuation at each step, yet listeners may still fail to recover this structure and treat other continuations as plausible. For instance, after observing an event such as A6, the true continuation in the sequence is C4. However, an imperfect listener may also consider an alternative, such as F4, plausible, consistent with the multi-step integration described above, in which events reachable after multiple steps are treated as if they were directly available next. Introducing such competing continuations increases the subjective uncertainty of the listener and alters the inferred transition structure from a single-outgoing edge pattern to a branching one. Conversely, in the pitch-class-only representation, the same

context reduces to A, for which both continuations C and F are in fact observed in the melody (i.e., A is followed by C and also by F). In that case, an error that mixes up which continuation occurred does not introduce a qualitatively new transition, but mainly shifts probability mass between already-available options (e.g., between $A \rightarrow C$ and $A \rightarrow F$), making the representation more robust to such perceptual errors. Therefore, understanding how topology modulates this perceptual error is necessary for evaluating which representations are more efficient for humans to use.

In short, representation choice fixes the transition statistics and therefore the distribution of uncertainty. Representing these statistics as a network makes their topology explicit. Because humans do not access transition statistics perfectly, perceptual constraints can make the same statistical uncertainty appear higher or lower, depending on how transitions are organized. This motivates (i) a systematic comparison of network structure across levels of representation detail and (ii) an analysis of how the resulting network topology relates to perceptual efficiency.

In this work, we address this issue by analysing eight network representations of music, drawing on and extending existing approaches in the literature. These vary in their level of detail, from single-feature encodings (pitch, interval, duration) to multi-feature combinations that incorporate octave or duration with pitch. We quantify how these representational choices reshape network topology and evaluate how efficiently each representation structures information by computing both the resulting entropy rate and the divergence from a perceptual-constraint estimate. Together, these measures make explicit a trade-off: increasing representational detail can preserve finer aspects of musical structure, but may produce a transition structure that is harder for humans to learn and use, while simpler encodings may sacrifice detail yet yield more perceptually efficient uncertainty estimates [20, 25]. In addition, by further examining how uncertainty and modeled error are distributed locally across each network representation—and how these patterns vary with piece length—we identify conditions under which random-walk centrality aligns with uncertainty. By quantifying how topology drives divergences between true transition statistics and a perceptually constrained estimate, our approach both reveals a representation-dependent bias that ideal-access expectation models can overlook [26, 27] and points toward incorporating realistic memory limits when relating uncertainty to neural [4] and behavioral data [28].

II. RESULTS

To examine how different levels of musical description shape structural and informational properties, we constructed eight network representations of the same sequences, spanning both established encodings from the

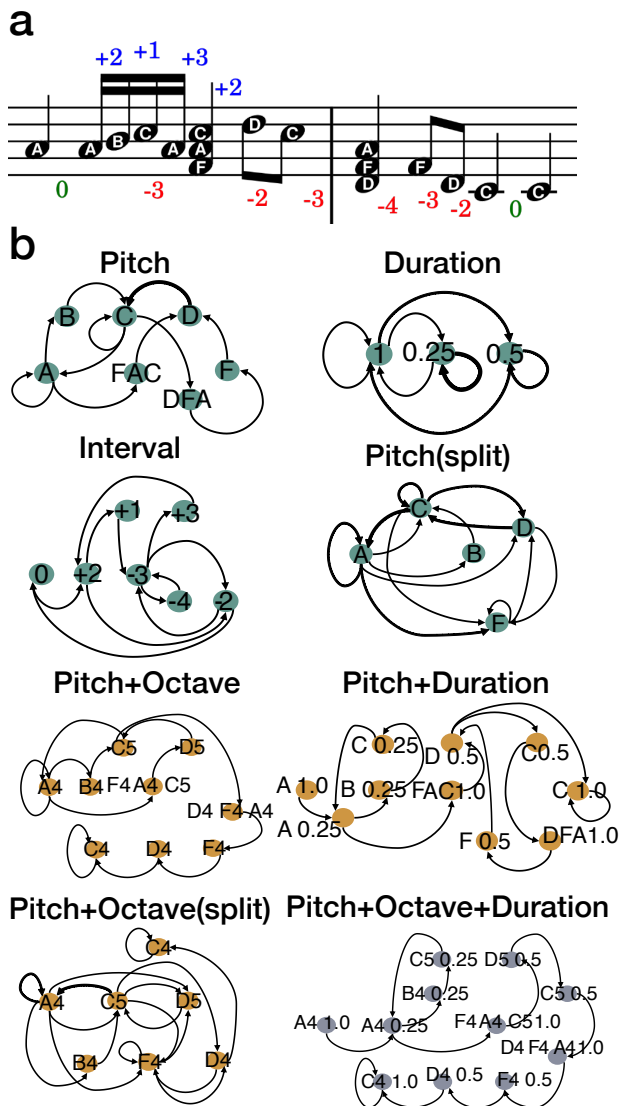


FIG. 1. **Networks reconstructed from a musical piece.** (a) A simple composition with highlighted interval changes. (b) Eight distinct network representations. All networks are directed and weighted: edges indicate transitions, and weights correspond to their frequencies.

literature and controlled feature-level variants introduced for systematic comparison. We start with minimal, single-feature encodings that expose the basic *building blocks* of musical structure, and then introduce additional features stepwise, allowing us to observe how topological and informational patterns emerge or transform as representational richness increases. In all cases, nodes correspond to unique feature configurations and edges record empirical transitions between consecutive elements in the musical sequence. The eight representations are defined as follows:

- *Pitch*: Each node represents the note being played, identified by its pitch class (e.g., C, D, E), without

distinguishing the octave. If several notes occur together (a chord), they form a single node [9].

- *Duration*: Each node represents how long a note or chord lasts, expressed as a standardized value relative to a beat.
- *Interval*: Each node represents the distance in semitones between two consecutive notes or chords (see Fig. 1a).
- *Pitch+Duration*: Each node represents the note or chord together with its duration.
- *Pitch+Octave*: Each node represents the note or chord together with its octave information.
- *Pitch+Duration+Octave*: Each node represents the note or chord with its duration and octave, combining all three features [6, 7].
- *Pitch (split)*: A variation of the *Pitch* model in which chords are split, so that each note is represented as a separate node. Edges are created from the predecessor to each note in the chord, and from each note to the possible successors.
- *Pitch+Octave (split)*: A variation of the *Pitch+Octave* model in which chords are split, with each note and its octave treated as a separate node. As in the previous model, edges connect the predecessor to each note in the chord and from each note to the possible successors [13, 14].

Given a musical piece in MIDI format, we constructed networks by tracking transitions between consecutive musical elements. Each transition forms a directed edge, while the definition of a node depends on the specific model chosen. The resulting networks are both *directed* and *weighted*, with edge weights corresponding to transition counts during the execution of the piece. Figure 1 illustrates the differences between the different representations. We detailed these differences in Supplementary Figure S1, which depicts network representations of Fryderyk Chopin’s Waltz in E-flat major, Op. 18.

In this work, we focus on piano compositions, which are both musically rich across multiple dimensions and well documented in large, curated corpora. Our corpus combines two sources: the piano-midi.de dataset [29], which contains 268 pieces, and the MSDM dataset [30], which contains 665 pieces. Together, these datasets cover works ranging from the Baroque period to the 20th century. We preprocessed and merged the two collections, separating the musical scores by left and right hands. Further details are provided in Methods Section IV A.

A. Structural consequences of representational choice

To assess the impact of the different model choices on network topology, we computed a range of undirected,

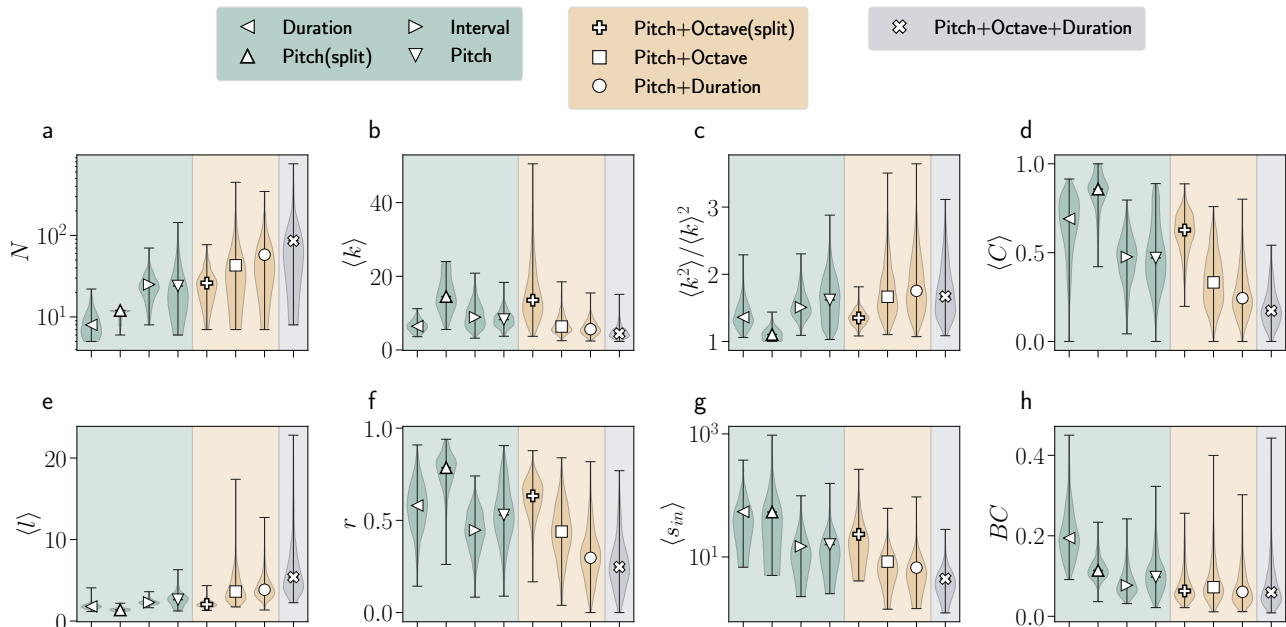


FIG. 2. **Topological properties of music network models.** Violin plots showing the distribution of eight network measures: (a) size N , (b) average degree $\langle k \rangle$, (c) degree heterogeneity $\langle k^2 \rangle / \langle k \rangle^2$, (d) average clustering coefficient $\langle C \rangle$, (e) average shortest path length $\langle l \rangle$, (f) reciprocity r , (g) average in-strength $\langle s_{in} \rangle$, and (h) betweenness centrality BC , across different models averaged over all musical pieces for the right hand. Models are grouped by the number of musical features used. Each symbol corresponds to an individual model and also highlights the median of each distribution.

directed, and weighted network measures for each representation (Supplementary Tables S1–S2). Figure 2 summarizes eight representative metrics for the right-hand networks. The smallest networks arise in the *Duration* and *Pitch(split)* models (Fig. 2a), whereas the *Pitch+Duration* and *Pitch+Octave+Duration* abstractions produce the largest and sparsest structures, with correspondingly low average degree (Fig. 2b), clustering coefficient (Fig. 2d), reciprocity (Fig. 2f), and betweenness centrality (Fig. 2h). In contrast, the *Pitch(split)* and *Pitch+Octave(split)* models yield the highest degrees and reciprocity, as splitting chords inflates local branching and introduces many short cycles. These contrasts illustrate how more compressed representations tend to concentrate transitions into dense, uniform structures, whereas adding descriptive features expands the state space and reveals finer organizational detail. Degree heterogeneity (Fig. 2c) remains low for the split models but increases systematically as additional features are incorporated, reflecting a controlled expansion of the state space, where new nodes increase in a structured manner and organize into progressively more diverse structural roles. Average shortest-path length (Fig. 2e) scales with network size across representations, while average in-strength (Fig. 2g) decreases inversely, since the same number of transitions is redistributed across more nodes. Additional metrics for left-hand networks show the same patterns (Supplementary Figs. S2–S4).

Collectively, these findings show that representational choices do not simply scale the size of the network but

reshape its structure in a systematic way. As additional musical features are incorporated, the state space expands in a way that networks become progressively more heterogeneous. This controlled expansion reflects how musical structure organizes itself across representational levels and highlights the distinctive regimes—dense, compressed configurations versus sparse and more heterogeneous ones—that different representations occupy.

B. Informational and perceptual effects of representational choice

Building on these topological patterns, we next examine how such structural differences influence the organization of musical information, shifting from network metrics to measures of information content. Following prior work [13], we examined how each representation organizes uncertainty by analyzing the Markov transition structure through the Shannon entropy of a random walk on the network [31, 32] (see Section IV B). Entropy here serves as a global measure of how the network channels—and restricts—possible continuations, providing a complementary perspective to the topological results above. It is computed by weighting each node’s local entropy, i.e., the uncertainty in its outgoing transitions, by the node’s stationary distribution:

$$S = \sum_i \pi_i S_i = - \sum_i \pi_i \sum_j P_{ij} \log P_{ij}, \quad (1)$$

where π_i denotes the stationary visitation probability of node i . This probability is calculated as the entries in the normalized eigenvector of the transition matrix \mathbf{P} , formed by the probabilities P_{ij} , corresponding to the eigenvalue 1, see details in Methods Section IV B. Because the stationary distribution reflects how often a diffusive random walker encounters each node in the long run, the resulting entropy captures how uncertainty is dynamically organized across the representation. In information-theoretic terms, it corresponds to the entropy rate or the average information produced per step of the encoded sequence.

Figure 3a shows that entropy varies systematically across representations, with simpler models generally exhibiting higher uncertainty and richer representations yielding lower average information per step. Duration is a notable exception: despite its simplicity, it exhibits relatively low entropy because it has a very small vocabulary and low average degree, which strongly constrains the set of possible continuations. As additional features are introduced, the vocabulary expands, and the networks become sparser (see Fig. 2a,b, and Supplementary Figure S5). Although a larger state space could, in principle, increase uncertainty, the added specificity makes many transitions more predictable, thereby lowering the average information produced per step. Importantly, this entropy reduction does not reflect a homogeneous decrease in uncertainty across all states.

Richer representations develop a pronounced heterogeneity (Fig. 2c). From an information perspective, this implies that many nodes have near-deterministic successors, whereas others act as hubs with multiple plausible continuations. By contrast, chord-splitting models inject extra local branching, inflating uncertainty despite using the same underlying musical material. This effect is evident when comparing *Pitch+Octave* versus *Pitch+Octave(split)* models, where splitting chords yields substantially higher entropy. To distinguish uncertainty due solely to connectivity from uncertainty influenced by empirical transition frequencies (i.e., how often each transition occurs in the corpus), Figure 3a also compares entropy in weighted versus unweighted networks. In the weighted case, transition probabilities P_{ij} are estimated from observed counts, whereas in the unweighted case we set all outgoing edges from a node to be equiprobable ($P_{ij} = 1/k_i^{out}$), recompute the stationary distribution π , and then evaluate Eq. (1). The largest discrepancy appears in the *Duration* model, where ignoring weights makes this highly compressed representation appear far more uncertain than it actually is.

To separate uncertainty arising from local node-level constraints from that produced by the global arrangement of transitions, we compared each representation with a degree- and out-strength-preserving null model (Rand A), which fixes the local entropies at each node. Any differences in global entropy therefore reflect how the stationary distribution reallocates weight across these unchanged local uncertainties. Across representa-

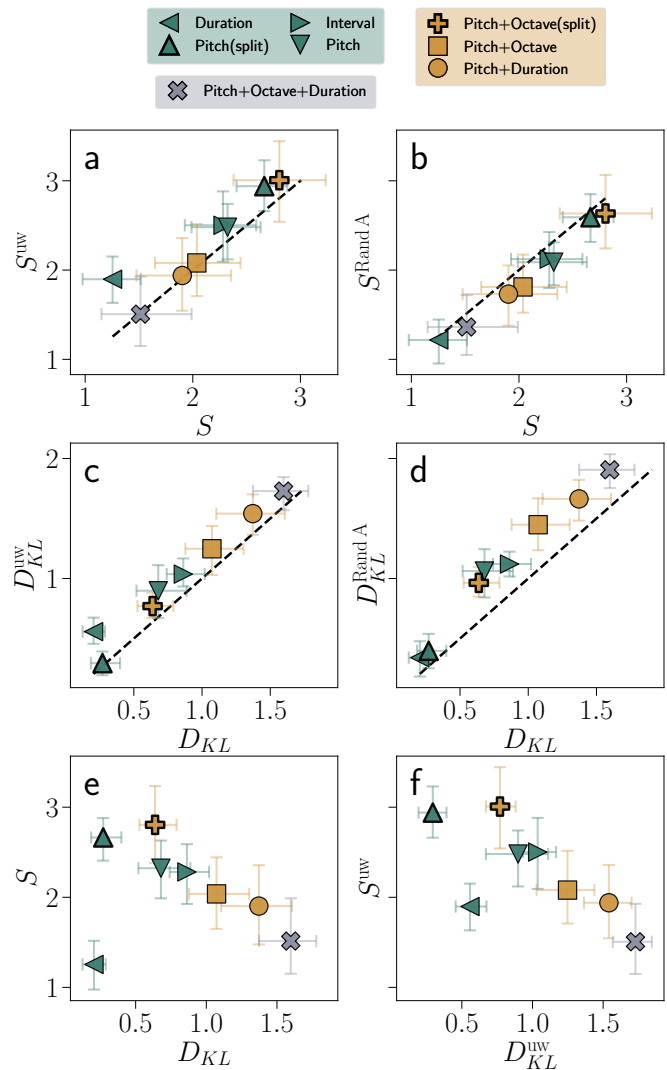


FIG. 3. **Information content and perception efficiency in music network models.** (a) Median entropy of weighted S versus unweighted S^{uw} networks. (b) Median entropy of type-A randomized networks S versus entropy of type-A randomized networks S^{RandA} . (c) Median Kullback-Leibler divergence of weighted D_{KL} versus unweighted D_{KL}^{uw} networks. (d) Median D_{KL} versus D_{KL} of type-A randomized networks. (e) Median D_{KL} versus median S . (f) Median D_{KL}^{uw} versus median S^{uw} . Models are grouped by the number of musical features used. Each symbol corresponds to an individual model. Error bars show the interquartile range (IQR) around the median.

tions—except for the most compressed ones (*Duration* and *Pitch(split)*), where structure is minimal—real networks consistently exhibit higher entropy than their randomized counterparts (Fig. 3b). This shows that visitation tends to concentrate in high-uncertainty regions, increasing the information produced per step beyond what the same local constraints would predict.

A second null model (Rand B), which randomizes edge weights while preserving the network skeleton, yields a comparable entropy reduction (Supplementary Figs. 6-

7), confirming that the specific placement of transition frequencies—not only the topology—plays a crucial role in shaping how uncertainty is distributed across a representation.

Uncertainty is tightly linked to the amount of perceptual effort involved in correctly tracking a musical sequence. Next, we quantify the perceptual difficulty of each representation, enabling us to assess how representational choices affect access to the encoded musical information. We use the framework developed by Lynn et al. in [20], which introduced a feature-agnostic model that estimates computationally the perceived transition structure under cognitive constraints. The model produces an inferred transition matrix $\hat{\mathbf{P}}$ from the true transition matrix,

$$\hat{\mathbf{P}} = (1 - \eta) \mathbf{P} (\mathbf{I} - \eta \mathbf{P})^{-1}, \quad (2)$$

which deviates from the true probabilities in ways consistent with empirically observed limitations due to inaccuracies, controlled by parameter η , and the integration of higher-order paths. To measure the deviation, we computed the KL divergence between the inferred transition matrix $\hat{\mathbf{P}}$ and the true matrix \mathbf{P} across representations. Lower divergence indicates that the perceptual model reconstructs the transition structure more faithfully, and thus that the representation communicates information more efficiently. See Methods Section IV C for more details.

KL divergence is lowest for single-feature models such as *Pitch* or *Duration*, and increases as additional features are combined, reaching its maximum in the *Pitch+Octave+Duration* model (Fig. 3c). In other words, simpler representations appear more perceptually efficient—they produce transition structures that are easier for the model to infer—even though they omit musically relevant distinctions. The strong performance of split models, however, should be interpreted with caution, as their artificially increased local branching makes them less sensitive to the smoothing applied in the perceptual estimate. Both null models confirm this pattern: for Rand A, KL divergence is consistently higher than in the real networks (Fig. 3d), except in the smallest representations, where real and randomized sequences are almost indistinguishable; Rand B yields a similar inflation (Supplementary Figures 6-7). Moreover, Figure 3c shows that, in line with results from Kulkarni et al. [13], incorporating edge weights consistently reduces KL divergence, confirming that empirical transition probabilities improve the alignment between the perceptual model and the true structure. This effect is most pronounced in the *Duration* representation, where weights seem to capture essential temporal information.

Taken together, the topological and information-theoretic results reveal a coherent progression across representational levels (Fig. 3e,f). Highly compressed, single-feature models produce smaller, denser networks with relatively uniform branching—a structure that yields high entropy per step but also low KL diver-

gence. These representations act as efficient communication channels: their limited state space and dense topology allow the perceptual model to reconstruct transition patterns with minimal error, even though the musical distinctions they encode are coarse. An exception is the *Duration* model, whose extremely small state space combined with heterogeneous edge weights yields low entropy, and whose KL divergence remains low because smoothing alters only a very limited set of transitions. As additional features are incorporated, network size grows, and connectivity becomes sparser and more heterogeneous. Degree variation increases, locally deterministic states emerge, and hubs with multiple continuations appear—topologies that concentrate information unevenly across the network. This controlled expansion lowers entropy because transitions become more specific, yet it simultaneously raises KL divergence, as the perceptual model struggles to approximate sharply peaked transition profiles. Therefore, the very structural refinement that enriches the representation creates a more challenging information landscape.

In combination, these patterns show that musical representations occupy a continuum between efficiency and descriptive detail. Compressed networks communicate information effectively but flatten musically relevant structure, whereas multi-feature networks preserve that structure at the cost of greater perceptual error. The topology of each representation—its size, branching patterns, and heterogeneity—largely determines where it sits along this continuum, clarifying how the choice of features reshapes both the organization of musical information and its accessibility under perceptual constraints.

C. Alignment of uncertainty and inference across musical representations

Building on the comparison of network representations, we now investigate how uncertainty and perception efficiency are organized within these networks. Specifically, we ask how entropy and perceptual errors are distributed along the network, how they vary with piece length, and how they manifest at the local level.

We first compare global entropy S with the average node entropy $\bar{S} = \frac{1}{N} \sum_i S_i$, which reflects node-level uncertainties without weighting by the stationary distribution. Across all models, \bar{S} is consistently lower than S (Fig. 4a), showing that high-entropy nodes receive more stationary mass. The increase in global entropy arises not only from degree heterogeneity but also from the alignment between stationary random-walk visitation and local uncertainty. This is evident from the out-strength-preserving null model (Rand A), which maintains the same heterogeneity yet shows lower entropy because this alignment is reduced (Fig. 3b). As a result, informational complexity becomes concentrated in a small set of frequently visited nodes. Left-hand results follow the same pattern (Supplementary Figure 6-7).

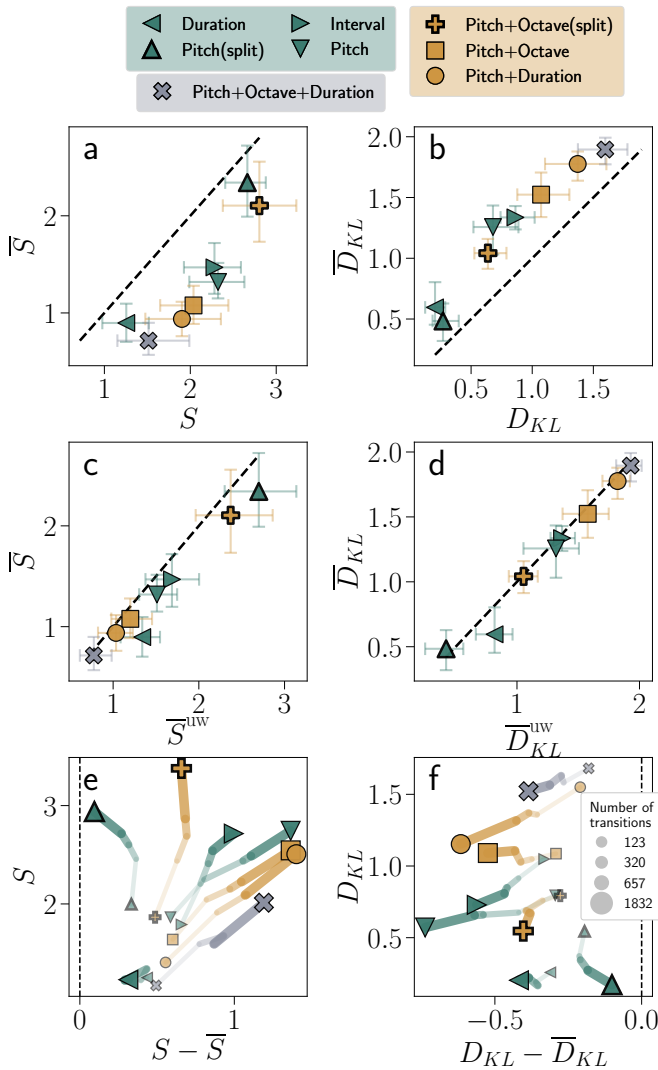


FIG. 4. **Global alignment of uncertainty and inference in music networks.** (a) Median entropy S versus mean node-level entropy \bar{S} . (b) Median KL divergence D_{KL} versus node-averaged KL divergence \bar{D}_{KL} . (c) Mean node-level entropy with and without edge weights (\bar{S} versus \bar{S}^{uw}). (d) Median node-averaged KL divergence with and without edge weights (\bar{D}_{KL} versus \bar{D}_{KL}^{uw}). (e) Median entropy S versus the difference between median and node-level entropy ($S - \bar{S}$). (f) Median KL divergence D_{KL} versus the difference between median and node-averaged KL divergence ($D_{KL} - \bar{D}_{KL}$). In (e) and (f) data is grouped by transition count. Transition counts are divided into five equal-sized bins. Smaller and more transparent markers correspond to shorter pieces. Points show medians, and error bars indicate the interquartile range. All panels correspond to right-hand tracks. Models are grouped by the number of musical features used. Each symbol corresponds to an individual model.

Next, we examine whether the inference model shows a similar alignment. The node-averaged KL divergence \bar{D}_{KL} , which ignores the stationary distribution (see Eq. 7), is consistently higher than the global D_{KL}

(Fig. 4b). Weighted and unweighted networks display nearly identical \bar{D}_{KL} values (Fig. 4d), showing that weights do not improve inference at individual states. Rather, they reshape the stationary distribution so that transitions easier for the inference model to approximate are visited more often. This pattern mirrors the entropy results and shows that stationary random-walk visitation naturally concentrates on transitions whose statistical structure aligns better with the perceptual model.

Then, we examine how this alignment varies with piece length. Global entropy increases with the number of transitions in a piece (Fig. 4e), whereas \bar{S} remains largely stable (Supplementary Figure 8a). Consequently, the gap $S - \bar{S}$ increases with length (Fig. 4e), meaning that high-entropy nodes absorb more stationary mass as pieces become longer. Chord-splitting models (*Pitch(split)*, *Pitch+Octave(split)*) show weaker alignment and a completely different evolution since uniformly high branching flattens the entropy landscape, and the *Duration* model shows a similar pattern due to its reduced structure.

The KL divergence shows a parallel trend. Global D_{KL} decreases slightly with length (Fig. 4f), while \bar{D}_{KL} remains stable (Supplementary Figure 8b), so the gap $D_{KL} - \bar{D}_{KL}$ increases (Fig. 4f). This indicates that longer pieces direct flow toward transitions that the inference model approximates well. The *Pitch(split)* model again deviates: its extreme compression causes networks to approach full connectivity as length increases, reducing structural distinctions and breaking the alignment between inference error and flow. In these cases, uncertainty remains high but loses meaningful organization, illustrating again how some modeling choices can result in degenerated structures. The two previous null models confirm that randomized networks exhibit weaker alignment and reduced length-dependent variation than the real data (Supplementary Figures 9-10).

Finally, to provide a more detailed perspective, we examine how these patterns manifest at the local level. To do so, we grouped nodes into quartiles according to their cumulative stationary distribution (π), with low-quartile nodes visited infrequently and high-quartile nodes visited more often. As shown in Figs. 5a,b, both short and long pieces exhibit a skewed visitation pattern: most nodes are rarely visited, while a small subset concentrates the majority of visitation mass. This effect becomes more pronounced in longer pieces and in multi-feature representations. Average node entropy \bar{S} is higher in high- π quartiles (Figs. 5c,d), while node-averaged KL divergence \bar{D}_{KL} is minimized in the same regions (Figs. 5e,f). This pattern confirms that uncertainty is concentrated in central, high- π nodes, while inference errors are relegated to the periphery. Because the stationary distribution is skewed, low-error central nodes dominate the overall inference, and high-error nodes carry little weight, demonstrating that the network structure itself mitigates the impact of the errors. This effect becomes even stronger in longer pieces, where the skew is more pronounced.

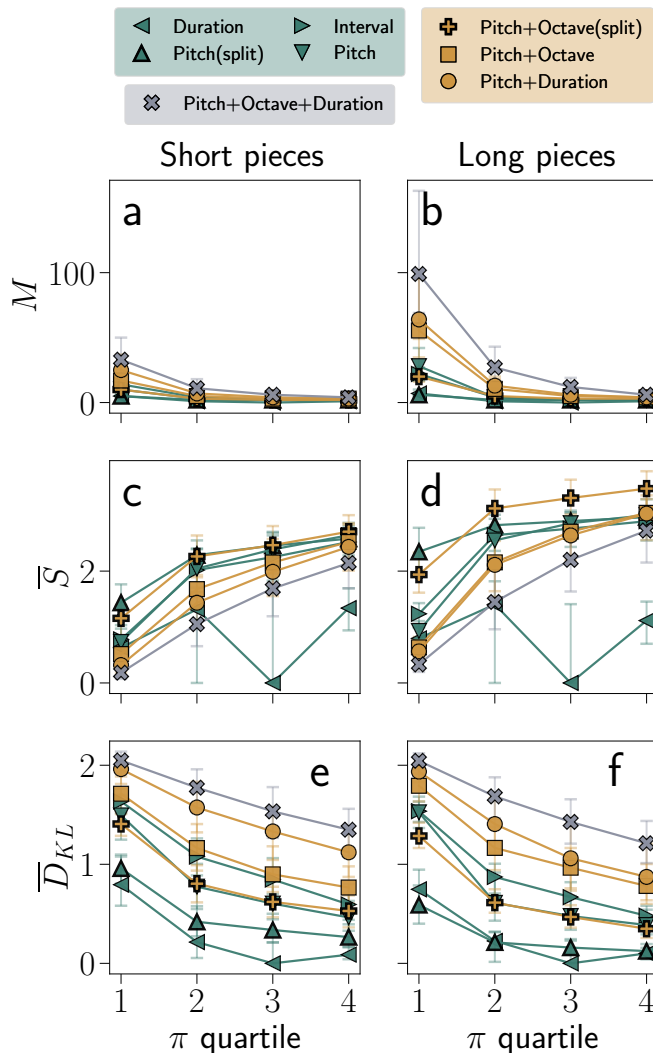


FIG. 5. **Local alignment of uncertainty and inference in music networks.** (a,b) Median fraction of nodes required to accumulate successive quartiles of stationary mass (M). (c,d) Average node entropy (\bar{S}) across π quartiles. (e,f) Node-averaged KL divergence (\bar{D}_{KL}) across π quartiles. Points denote medians and error bars show interquartile ranges. Columns separate short and long musical compositions, defined by dividing pieces into two equal bins by the number of transitions. All panels correspond to right-hand tracks. Models are grouped by the number of musical features used. Each symbol corresponds to an individual model.

Overall, these results show that musical networks align uncertainty and effective inference with the visitation frequency, and that this alignment strengthens with piece length. As additional features expand the state space, these landscapes become more pronounced: uncertainty concentrates in dynamically central states while inference errors diminish in regions carrying more weight. This progression reflects the emergence of efficient, heterogeneous structures that maintain coherence as representational detail increases and, in doing so, provide a land-

scape that facilitates the extraction of recurrent patterns.

III. DISCUSSION

Representational choice plays a decisive role in the structural properties of musical networks. Our results show that the number and grouping of features—and whether musical events are split or not—substantially influence the resulting topology. Properties often associated with musical corpora, such as small-world organization [6, 7], heavy-tailed degree distributions, or Zipf- and Heaps-like scaling [11, 16], emerge only under certain representational levels and are not inherent to the raw data alone. More detailed, multi-feature representations tend to produce markedly heterogeneous and skewed structures, whereas compressed vocabularies attenuate these patterns. These findings show that topological regularities in music depend on the definition of the underlying symbolic space.

Building on this, our results frame representational differences as a trade-off between descriptive richness and communication efficiency under perceptual constraints. Here, descriptive richness denotes the number of musically relevant distinctions preserved by an encoding. This determines how large and how fine-grained its event vocabulary (state space) is. A richer encoding typically makes one-step transitions more specific and more locally predictable, i.e., it lowers uncertainty. However, it can also make the transition structure harder to learn reliably. By contrast, communication efficiency refers to how well a listener can recover and use the resulting transition statistics. This assumes the listener has limited memory and only noisy access to the sequence. Compressed representations tend to yield lower perceptual error, suggesting that their transition topology can be tracked relatively well even with limited access to transition statistics. By contrast, richer representations that preserve finer details reshape the state space and introduce more complex transition structures, increasing the mismatch between true and constrained transition estimates and, in turn, reducing communication efficiency. This echoes principles from information bottleneck theory [25] and minimum-description-length formulations [33], in which representations balance fidelity against cognitive cost. In our network framework, this cost becomes explicit: the representation choice determines not only the information carried per step (entropy rate) but also the structural accessibility of that information, quantified by the divergence between the true transition matrix and its cognitively constrained approximation. Viewed this way, representational choices and perceptual limitations jointly determine the uncertainty a listener effectively experiences.

Although our analysis remains descriptive rather than cognitive, the emergence of efficient communication channels in simpler representations parallels several known properties of auditory and musical processing. Neural

pathways handle pitch, duration, and timbre through partially distinct streams [34], and hierarchical integration [35, 36] resembles the progressive increase in structural complexity we observe as more features are added. At the same time, human expectations depend on learning and exposure [27, 37], and thus cannot be reduced to the statistical transitions of the piece under study. Our results, therefore, do not model cognition directly, but they provide a structural account of how musical information is organized and of the cost of accessing it. State-of-the-art models of these musical expectations [26] estimate uncertainty directly from learned transitions, implicitly assuming ideal access to prior musical exposure in memory. In this work, we use network representations to make explicit how imperfect access to transition statistics reshapes uncertainty, and to quantify how this effect depends on representational choice by measuring the topology-dependent gap between true and constrained transition estimates. Therefore, a natural extension of this work is to examine how expectations derived from these statistical-learning models interact with the informational landscapes uncovered here.

This structural organization also offers insight into why some musical systems support pattern discovery more effectively than others [14]. In richer representations, uncertainty concentrates in dynamically central nodes, whereas less central nodes remain relatively predictable. Such landscapes provide learners with stable contexts and informative deviations, a contrast to uniformly uncertain or near-random systems in which motifs and regularities become difficult to extract. Notably, this interplay between predictable structure and localized surprise has also been linked to affective responses in music, where heterogeneous uncertainty can enhance engagement and pleasure [3, 28, 38]. Although learning is beyond the scope of this work, the results suggest that differentiated uncertainty may facilitate both pattern extraction and the perception of structure in musical sequences.

Our representational hierarchy was chosen to build on established symbolic viewpoints in music-network research while enabling a controlled progression from coarse to detailed descriptions. Other musically informed viewpoints—such as tonality-relative encodings based on scale degree or harmonic function (e.g., tonic/dominant), or learned feature spaces—may yield different structural signatures and should be explored in future work. Similarly, our focus on classical piano music provided a rich context for examining how complexity grows with representational detail, but the same framework can be applied to other repertoires. Our intuition is that genres with more repetitive or minimalist structures will show weaker differentiation across representational levels, offering a useful contrast to the dynamics observed here.

More broadly, this approach demonstrates how the structural and informational consequences of representational choice can be analyzed in any sequential domain. Music serves as a clear testbed because its feature combinations and hierarchical abstractions are well-

characterized, yet the framework is readily transferable to other sequences and systems. By tracing how topologies and informational landscapes evolve with representational detail, we gain a principled way to compare how different feature sets shape the organization of sequential information and the emergence of efficient heterogeneous structures.

IV. METHODS

A. Datasets and Preprocessing

We used two publicly available collections of piano music in MIDI format: the piano-midi.de dataset [29] (268 pieces) and the MSDM dataset [30] (665 pieces). After merging, the corpus comprised 933 files spanning works from the Baroque to the 20th century. Some duplicates remain, since different encodings of the same composition may capture distinct transcription choices.

MIDI files were selected only if they included tempo and time-signature metadata to ensure accurate quantization of durations. We further restricted the corpus to files containing exactly two tracks, corresponding to the left and right hands of a piano score. Each track was converted into a directed and weighted network, resulting in two networks for each composition. To ensure a well-defined entropy with a unique stationary distribution, we restrict our analysis to the largest strongly connected component (LSCC) of each network. Moreover, to ensure that the resulting networks faithfully represented the musical pieces, we retained only LSCCs that contained at least 80% of the nodes, yielding more than 600 networks per model.

During preprocessing, each musical element was encoded according to the chosen network representation (see Section II). Symbolic features include pitch (frequency, grouped into pitch classes an octave apart), duration (quantized relative to a quarter note = 1.0), and chromatic interval (pitch distance in semitones between consecutive events). If multiple pitches occurred simultaneously, the highest pitch was used to compute intervals. Descriptive statistics on pitch ranges, note durations, chord distributions, and interval patterns for both datasets, including systematic differences between left and right hands, are provided in Supplementary Section IV.

B. Entropy in complex networks

The Shannon entropy for a node i can be written as [13, 31]

$$S_i = - \sum_j P_{ij} \log P_{ij}, \quad (3)$$

where P_{ij} are the entries of the transition matrix \mathbf{P} . In the case of directed and weighted networks, $P_{ij} =$

$\omega_{ij}/s_i^{\text{out}}$, where ω_{ij} is the edge weight and s_i^{out} is the out-strength of the node i . Here we consider only outgoing links from node i . In unweighted networks, the out-strength is replaced by the out-degree k_i^{out} .

The entropy of the entire network has the form of Eq. 1. The stationary distribution π satisfies the condition $\mathbf{P}\pi = \pi$ and can be obtained as the normalized eigenvector of \mathbf{P} corresponding to the eigenvalue 1. For the simplest case, i.e., an undirected and unweighted graph, the stationary distribution becomes $\pi_i = k_i/2E$ where k_i is the degree of node i and E is the total number of edges. It is worth noting that the formula is only applicable when a network has a single strongly connected component. In the preprocessing step, we ensure that we work with such networks.

C. Human perception model

We adopt the human perception model introduced by Lynn et al. [21], which we briefly summarize here for completeness, as it serves as the basis for our perceptual analysis. In this model, the inferred transition probabilities $\hat{\mathbf{P}}$ are expressed in terms of the true transition probabilities \mathbf{P} as

$$\hat{\mathbf{P}} = (1 - \eta) \mathbf{P} (\mathbf{I} - \eta \mathbf{P})^{-1}, \quad (4)$$

where $\eta \in [0, 1]$ controls the inaccuracy of perceptual expectations, and $(\mathbf{I} - \eta \mathbf{P})^{-1}$ denotes a *matrix inverse*. This inverse can be expanded as a geometric series,

$$(\mathbf{I} - \eta \mathbf{P})^{-1} = \sum_{t=0}^{\infty} (\eta \mathbf{P})^t, \quad (5)$$

which reveals that perception integrates not only direct (one-step) transitions but also higher-order paths—two, three, or more steps apart—each weighted by a decaying factor η^t . Consequently, $\hat{\mathbf{P}}$ represents a temporally smoothed higher-order estimate of the transition structure. Empirical evidence suggests an average human accuracy parameter of $\eta \approx 0.8$ which we use for our computation [20].

To quantify the discrepancy in the perception of music networks, i.e., the difference between these two probabilities, we use the Kullback-Leibler (KL) divergence defined as:

$$D_{KL}(\mathbf{P} \parallel \hat{\mathbf{P}}) = - \sum_i \pi_i \sum_j P_{ij} \log \frac{\hat{P}_{ij}}{P_{ij}}. \quad (6)$$

The lower the KL divergence, the smaller the difference between \mathbf{P} and $\hat{\mathbf{P}}$. In addition, we define the uniform average of the KL divergence as

$$\bar{D}_{KL}(\mathbf{P} \parallel \hat{\mathbf{P}}) = - \frac{1}{N} \sum_{i=1}^N \sum_j P_{ij} \log \frac{\hat{P}_{ij}}{P_{ij}}. \quad (7)$$

ACKNOWLEDGMENTS

We thank Timoteo Carletti and Nicolás Bono Rosselló for helpful comments and feedback on the manuscript. L. B. R and R. J acknowledge support from the Bridge grant funded by Young Researchers of the Complex Systems Society (yrCSS). R. J. acknowledges support from the fellowship FIDUR funded by Generalitat de Catalunya. L. B. R acknowledges support from the ARIAC project (No. 2010235), funded by the Service Public de Wallonie (SPW Recherche). M. A. S and M. B. acknowledge support from grant PID2022-137505NB-C22 funded by MCIN/AEI/10.13039/501100011033 and by “ERDF/EU”. M. B. acknowledges the ICREA Academia award, funded by the Generalitat de Catalunya.

V. DATA AVAILABILITY

The network datasets used in this study are available from the sources referenced in the manuscript and the supplementary materials.

VI. CODE AVAILABILITY

To generate the different network models, we have produced software that allows us to read MIDI files from the given datasets, select the features that will be used to build the given model, and produce the graphs for each track in the MIDI file, together with a text file that corresponds to the given viewpoint sequence. We will provide an open-source code upon publication.

-
- [1] S. Koelsch, *Nature reviews neuroscience* **15**, 170 (2014).
- [2] S. Koelsch, P. Vuust, and K. Friston, *Trends in cognitive sciences* **23**, 63 (2019).
- [3] V. K. Cheung, P. M. Harrison, L. Meyer, M. T. Pearce, J.-D. Haynes, and S. Koelsch, *Current Biology* **29**, 4084 (2019).
- [4] E. Mas-Herrero and J. Marco-Pallarés, *Proceedings of the National Academy of Sciences* **122**, e2500494122 (2025).
- [5] D. Conklin and I. H. Witten, *Journal of New Music Research* **24**, 51 (1995).
- [6] X. Liu, C. K. Tse, and M. Small, *Lecture Notes of the Institute for Computer Sciences, Social Informatics and Telecommunications Engineering Complex Sciences*, 2196–2205 (2009).
- [7] S. Ferretti, Springer Science+Business Media (2017).
- [8] F. Gomez, T. Lorimer, and R. Stoop, *Nonlinear Dynamics of Electronic Systems Communications in Computer and Information Science*, 262–269 (2014).
- [9] J. Serrà, A. Corral, M. Boguñá, M. Haro, and J. L. Arcos, *Scientific Reports* **2** (2012), 10.1038/srep00521.
- [10] M. B. Nardelli, *Journal of Mathematics and Music* **17**, 198 (2023).
- [11] B. Manaris, J. Romero, P. Machado, D. Krehbiel, T. Hirzel, W. Pharr, and R. B. Davis, *Computer Music Journal* **29**, 55 (2005).
- [12] M. Serra-Peralta, J. Serrà, and Á. Corral, *EPJ Data Science* **10**, 40 (2021).
- [13] S. Kulkarni, S. U. David, C. W. Lynn, and D. S. Bassett, *Physical Review Research* **6**, 013136 (2024).
- [14] N. Di Marco, E. Loru, A. Galeazzi, M. Cinelli, and W. Quattrociochi, arXiv preprint arXiv:2501.07557 (2025).
- [15] M. B. del Río, G. Cocho, and G. Naumis, *Physica A: Statistical Mechanics and its Applications* **387**, 5552 (2008).
- [16] D. H. Zanette, *Musicae Scientiae* **10**, 3 (2006).
- [17] F. C. Moss, M. Neuwirth, D. Harasim, and M. Rohrmeier, *PLoS One* **14**, e0217242 (2019).
- [18] S. A. Mehr, M. Singh, D. Knox, D. M. Ketter, D. Pickens-Jones, S. Atwood, C. Lucas, N. Jacoby, A. A. Egner, E. J. Hopkins, *et al.*, *Science* **366**, eaax0868 (2019).
- [19] M. Rohrmeier and I. Cross, in *Proceedings of the 10th international conference on music perception and cognition*, Vol. 6 (ICMPC Sapporo, 2008) pp. 123–1319.
- [20] C. W. Lynn, L. Papadopoulos, A. E. Kahn, and D. S. Bassett, *Nature Physics* **16**, 965 (2020).
- [21] C. W. Lynn, A. E. Kahn, N. Nyema, and D. S. Bassett, *Nature communications* **11**, 2313 (2020).
- [22] I. Momennejad, E. M. Russek, J. H. Cheong, M. M. Botvinick, N. D. Daw, and S. J. Gershman, *Nature human behaviour* **1**, 680 (2017).
- [23] M. W. Howard and M. J. Kahana, *Journal of mathematical psychology* **46**, 269 (2002).
- [24] F. Meyniel, M. Maheu, and S. Dehaene, *PLoS computational biology* **12**, e1005260 (2016).
- [25] N. Tishby, F. C. Pereira, and W. Bialek, arXiv preprint physics/0004057 (2000).
- [26] M. T. Pearce and G. A. Wiggins, *Topics in cognitive science* **4**, 625 (2012).
- [27] M. T. Pearce, *Annals of the New York Academy of Sciences* **1423**, 378 (2018).
- [28] B. P. Gold, M. T. Pearce, E. Mas-Herrero, A. Dagher, and R. J. Zatorre, *Journal of Neuroscience* **39**, 9397 (2019).
- [29] B. Krueger, “Piano midi,” (1996–2018).
- [30] M. Dorfer, j. Hajič, Jan, A. Arzt, H. Frostel, and G. Widmer, “Msmmd - multimodal sheet music dataset,” (2019).
- [31] J. Gómez-Gardenes and V. Latora, *Physical Review E—Statistical, Nonlinear, and Soft Matter Physics* **78**, 065102 (2008).
- [32] C. E. Shannon, *The Bell system technical journal* **27**, 379 (1948).
- [33] J. Rissanen, *The Annals of statistics* **11**, 416 (1983).
- [34] I. Peretz and M. Coltheart, *Nature neuroscience* **6**, 688 (2003).
- [35] I. Peretz and R. J. Zatorre, *Annu. Rev. Psychol.* **56**, 89 (2005).
- [36] S. Koelsch, *Frontier in Psychology* **2**, 110 (2011).
- [37] T. Daikoku, G. A. Wiggins, and Y. Nagai, *Frontiers in Neuroscience* **15**, 640412 (2021).
- [38] D. Huron, *Sweet anticipation: Music and the psychology of expectation* (MIT press, 2008).

Supplementary Information for “Trade-offs between structural richness and communication efficiency in music network representations”

Lluc Bono Rosselló,¹ Robert Jankowski,^{2,3,4} Hugues Bersini,¹ Marián Boguñá,^{3,4} and M. Ángeles Serrano^{3,4,5}

¹*Institute for Interdisciplinary Studies on Artificial Intelligence (IRIDIA),
Université Libre de Bruxelles, Brussels, Belgium*

²*Faculty of Electrical Engineering, Mathematics and Computer Science,
Delft University of Technology, 2628 CD, Delft, Netherlands*

³*Departament de Física de la Matèria Condensada,
Universitat de Barcelona, Martí i Franquès 1, E-08028 Barcelona, Spain*

⁴*Universitat de Barcelona Institute of Complex Systems (UBICS), Universitat de Barcelona, Barcelona, Spain*

⁵*ICREA, Passeig Lluís Companys 23, E-08010 Barcelona, Spain*

(Dated: March 11, 2026)

CONTENTS

I. Example network representations of Fryderyk Chopin’s piece	2
II. Network properties	3
III. Information content and perception efficiency in music networks	7
IV. Descriptive analysis of the datasets	10

I. EXAMPLE NETWORK REPRESENTATIONS OF FRYDERYK CHOPIN'S PIECE

Figure S1 presents eight different network representations of Fryderyk Chopin's Waltz in E-flat major, Op. 18. The *Duration* model results in the smallest network, reflecting the limited set of distinct note durations. In contrast, the *Pitch(split)* model is only based on 12 possible pitches. As anticipated, the *Pitch+Octave+Duration* model produces the largest network, characterized by only a few self-loops. These observations underscore the variability inherent in different network representations of the same musical piece

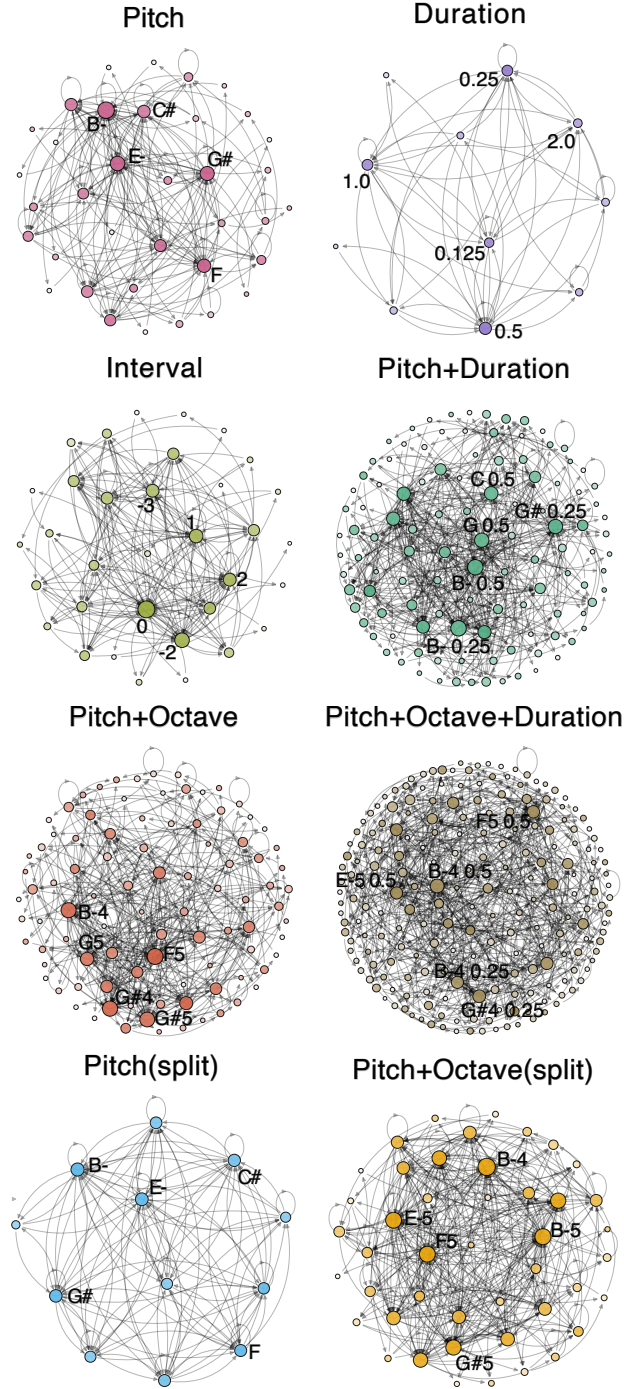


FIG. S1: Different network representations of Waltz in E-flat major, Op. 18 by Fryderyk Chopin. All networks are directed and weighted. The size of the nodes is proportional to their degree.

II. NETWORK PROPERTIES

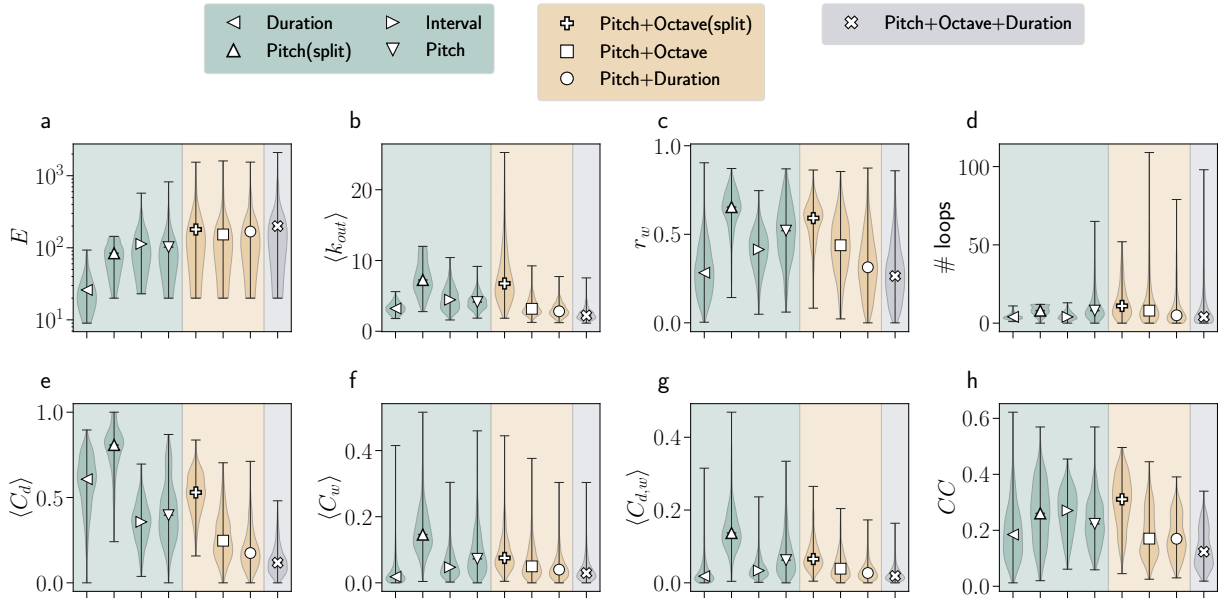


FIG. S2: Violin plots showing the distribution of eight network measures— (a) number of edges E , (b) average out-degree $\langle k_{out} \rangle$, (c) weighted reciprocity r_w , (d) number of self-loops $\# \text{ loops}$, (e) average directed and weighted clustering coefficient $\langle C_d \rangle$, (f) average undirected and weighted clustering coefficient $\langle C_w \rangle$, (g) average directed and weighted clustering coefficient $\langle C_{d,w} \rangle$, and (h) closeness centrality CC —across different models averaged over all music pieces for the **right** hand. Models are grouped by the number of musical features used. Each symbol corresponds to an individual model and also highlights the median of each distribution.

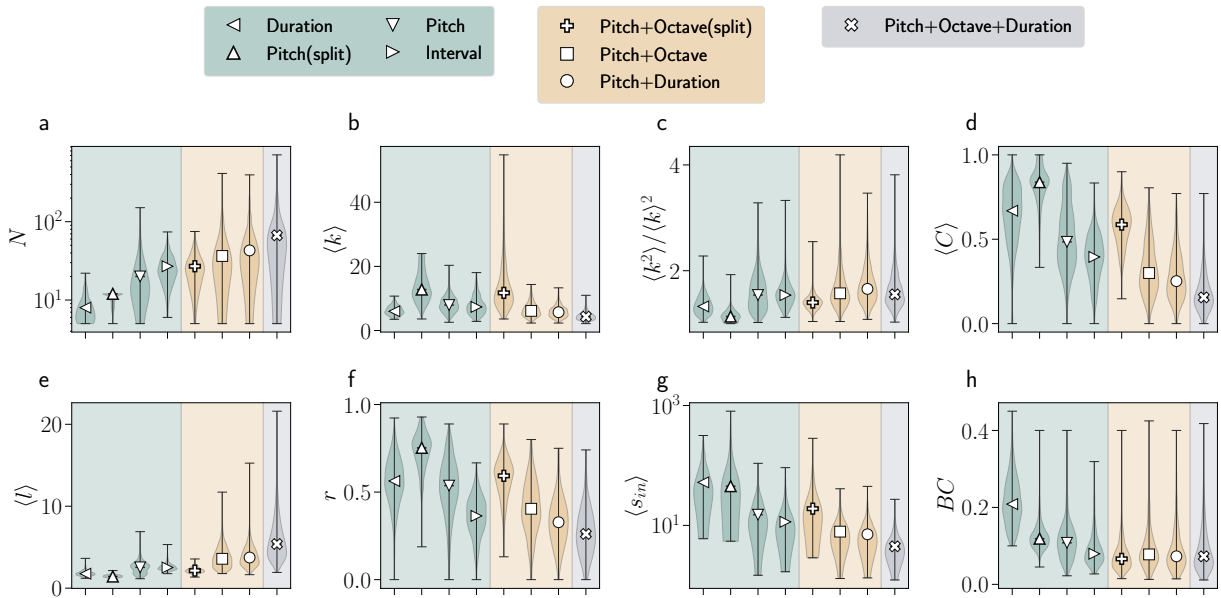


FIG. S3: Violin plots showing the distribution of eight network measures: (a) size N , (b) average degree $\langle k \rangle$, (c) degree heterogeneity $\langle k^2 \rangle / \langle k \rangle^2$, (d) average clustering coefficient $\langle C \rangle$, (e) average shortest path length $\langle l \rangle$, (f) reciprocity r , (g) average in-strength $\langle s_{in} \rangle$, and (h) betweenness centrality BC , across different models averaged over all music pieces for the **left** hand. Models are grouped by the number of musical features used. Each symbol corresponds to an individual model and also highlights the median of each distribution.

TABLE S1: **Network metrics averaged by model.** Size N , number of edges E , average degree $\langle k \rangle$, reciprocity r , weighted reciprocity r_w , number of self-loops $\#$ loops, average undirected and unweighted clustering coefficient $\langle C \rangle$, average directed and weighted clustering coefficient $\langle C_d \rangle$, average undirected and weighted clustering coefficient $\langle C_w \rangle$, average directed and weighted clustering coefficient $\langle C_{d,w} \rangle$, average out-degree $\langle k_{out} \rangle$, degree heterogeneity $\langle k^2 \rangle / \langle k \rangle^2$, average in-strength $\langle s_{in} \rangle$, average shortest path length $\langle l \rangle$, closeness centrality CC , betweenness centrality BC , weighted entropy S and weighted KL-divergence, across different models averaged over all music pieces for the right hand.

Model	Duration	Interval	Pitch	Pitch+Duration	Pitch+Octave	Pitch+Octave+Duration	Pitch+Octave(split)	Pitch(split)
N	9.04 ± 3.40	26.40 ± 9.06	30.28 ± 21.07	72.95 ± 54.16	64.66 ± 64.09	118.77 ± 110.25	28.34 ± 12.08	10.99 ± 1.49
E	30.83 ± 17.14	132.35 ± 81.58	128.82 ± 103.53	222.66 ± 191.07	211.85 ± 201.21	279.73 ± 264.41	253.26 ± 233.70	84.62 ± 33.11
$\langle k \rangle$	6.50 ± 1.51	9.33 ± 3.12	8.46 ± 2.28	5.95 ± 1.82	6.89 ± 2.29	4.76 ± 1.49	15.39 ± 7.56	14.97 ± 4.68
r	0.57 ± 0.13	0.44 ± 0.11	0.53 ± 0.14	0.30 ± 0.14	0.43 ± 0.14	0.26 ± 0.14	0.62 ± 0.10	0.77 ± 0.09
r_w	0.29 ± 0.14	0.41 ± 0.11	0.51 ± 0.16	0.32 ± 0.17	0.43 ± 0.16	0.28 ± 0.16	0.58 ± 0.11	0.65 ± 0.11
$\#$ loops	3.99 ± 1.66	4.71 ± 2.42	10.81 ± 9.45	8.67 ± 10.33	13.17 ± 15.77	8.39 ± 11.70	13.75 ± 10.54	7.99 ± 3.01
$\langle C \rangle$	0.65 ± 0.17	0.47 ± 0.13	0.49 ± 0.18	0.26 ± 0.13	0.34 ± 0.15	0.19 ± 0.10	0.62 ± 0.11	0.84 ± 0.10
$\langle C_d \rangle$	0.58 ± 0.17	0.35 ± 0.12	0.42 ± 0.17	0.19 ± 0.11	0.27 ± 0.13	0.13 ± 0.08	0.52 ± 0.12	0.79 ± 0.12
$\langle C_w \rangle$	0.03 ± 0.04	0.06 ± 0.04	0.09 ± 0.06	0.05 ± 0.04	0.06 ± 0.05	0.04 ± 0.03	0.09 ± 0.05	0.16 ± 0.07
$\langle C_{d,w} \rangle$	0.03 ± 0.03	0.04 ± 0.03	0.07 ± 0.05	0.03 ± 0.03	0.05 ± 0.03	0.02 ± 0.02	0.07 ± 0.04	0.15 ± 0.06
$\langle k_{out} \rangle$	3.25 ± 0.76	4.67 ± 1.56	4.23 ± 1.14	2.97 ± 0.91	3.45 ± 1.15	2.38 ± 0.74	7.70 ± 3.78	7.49 ± 2.34
$\langle k^2 \rangle / \langle k \rangle^2$	1.39 ± 0.19	1.54 ± 0.19	1.63 ± 0.32	1.83 ± 0.40	1.74 ± 0.37	1.74 ± 0.39	1.35 ± 0.11	1.11 ± 0.08
$\langle s_{in} \rangle$	72.66 ± 60.96	20.59 ± 16.36	20.76 ± 17.33	8.40 ± 7.33	10.26 ± 7.00	5.25 ± 3.30	35.96 ± 32.49	107.96 ± 134.90
$\langle l \rangle$	1.80 ± 0.27	2.32 ± 0.27	2.64 ± 0.74	4.12 ± 1.29	4.08 ± 1.88	6.31 ± 3.24	2.11 ± 0.36	1.36 ± 0.20
CC	0.19 ± 0.10	0.27 ± 0.08	0.23 ± 0.08	0.18 ± 0.07	0.19 ± 0.09	0.14 ± 0.07	0.30 ± 0.09	0.26 ± 0.11
BC	0.20 ± 0.06	0.08 ± 0.03	0.10 ± 0.04	0.07 ± 0.04	0.08 ± 0.05	0.07 ± 0.05	0.07 ± 0.04	0.12 ± 0.03
S	1.23 ± 0.40	2.27 ± 0.46	2.29 ± 0.44	1.91 ± 0.58	2.05 ± 0.52	1.57 ± 0.57	2.80 ± 0.62	2.60 ± 0.39
D_{KL}	0.23 ± 0.15	0.89 ± 0.23	0.73 ± 0.27	1.35 ± 0.35	1.10 ± 0.29	1.58 ± 0.29	0.67 ± 0.20	0.31 ± 0.17

TABLE S2: **Network metrics averaged by model.** Topological properties across different models averaged over all music pieces for the left hand. See Table S1 for more details.

Model	Duration	Interval	Pitch	Pitch+Duration	Pitch+Octave	Pitch+Octave+Duration	Pitch+Octave(split)	Pitch(split)
N	8.47 ± 3.46	29.15 ± 11.12	25.69 ± 18.4	58.16 ± 47.76	53.79 ± 49.44	94.99 ± 91.08	29.1 ± 12.3	10.81 ± 1.62
E	27.74 ± 16.02	124.51 ± 87.99	106.3 ± 88.39	174.46 ± 157.25	174.65 ± 167.35	215.4 ± 206.98	230.63 ± 225.19	76.38 ± 32.91
$\langle k \rangle$	6.28 ± 1.45	7.84 ± 2.87	8.16 ± 2.45	5.87 ± 1.81	6.45 ± 2.12	4.53 ± 1.3	13.56 ± 7.06	13.68 ± 4.68
r	0.56 ± 0.13	0.36 ± 0.11	0.53 ± 0.16	0.33 ± 0.14	0.41 ± 0.15	0.27 ± 0.14	0.57 ± 0.12	0.73 ± 0.11
r_w	0.26 ± 0.14	0.32 ± 0.14	0.49 ± 0.17	0.35 ± 0.18	0.42 ± 0.18	0.3 ± 0.18	0.54 ± 0.14	0.6 ± 0.12
# loops	4.09 ± 1.69	4.23 ± 2.52	10.26 ± 9.67	9.79 ± 11.24	11.05 ± 14.7	7.94 ± 12.39	11.89 ± 10.3	7.55 ± 3.01
$\langle C \rangle$	0.64 ± 0.18	0.39 ± 0.13	0.5 ± 0.19	0.28 ± 0.14	0.32 ± 0.15	0.18 ± 0.11	0.57 ± 0.11	0.82 ± 0.11
$\langle C_d \rangle$	0.56 ± 0.18	0.27 ± 0.11	0.43 ± 0.18	0.2 ± 0.12	0.24 ± 0.13	0.12 ± 0.08	0.48 ± 0.12	0.76 ± 0.13
$\langle C_w \rangle$	0.03 ± 0.03	0.05 ± 0.04	0.09 ± 0.07	0.05 ± 0.05	0.06 ± 0.05	0.04 ± 0.04	0.08 ± 0.05	0.14 ± 0.07
$\langle C_{d,w} \rangle$	0.03 ± 0.03	0.03 ± 0.02	0.08 ± 0.06	0.04 ± 0.03	0.04 ± 0.04	0.02 ± 0.02	0.07 ± 0.04	0.13 ± 0.06
$\langle k_{out} \rangle$	3.14 ± 0.72	3.92 ± 1.44	4.08 ± 1.23	2.93 ± 0.9	3.22 ± 1.06	2.26 ± 0.65	6.78 ± 3.53	6.84 ± 2.34
$\langle k^2 \rangle / \langle k \rangle^2$	1.35 ± 0.18	1.57 ± 0.24	1.58 ± 0.33	1.72 ± 0.34	1.65 ± 0.34	1.62 ± 0.32	1.4 ± 0.13	1.14 ± 0.11
$\langle s_{in} \rangle$	70.9 ± 56.98	15.08 ± 12.2	18.63 ± 13.11	8.3 ± 5.39	9.14 ± 5.52	5.27 ± 3.31	30.7 ± 31.75	93.74 ± 121.57
$\langle l \rangle$	1.81 ± 0.32	2.59 ± 0.41	2.53 ± 0.74	3.94 ± 1.31	3.82 ± 1.35	5.99 ± 2.63	2.2 ± 0.35	1.42 ± 0.21
CC	0.2 ± 0.1	0.24 ± 0.08	0.24 ± 0.09	0.19 ± 0.08	0.19 ± 0.09	0.14 ± 0.07	0.3 ± 0.09	0.27 ± 0.11
BC	0.22 ± 0.06	0.09 ± 0.04	0.11 ± 0.05	0.09 ± 0.06	0.09 ± 0.06	0.09 ± 0.06	0.07 ± 0.04	0.12 ± 0.03
S	1.1 ± 0.4	1.97 ± 0.52	2.16 ± 0.49	1.81 ± 0.53	1.88 ± 0.54	1.43 ± 0.51	2.65 ± 0.63	2.47 ± 0.4
D_{KL}	0.23 ± 0.14	1.1 ± 0.27	0.69 ± 0.26	1.23 ± 0.32	1.16 ± 0.27	1.52 ± 0.29	0.76 ± 0.25	0.33 ± 0.17

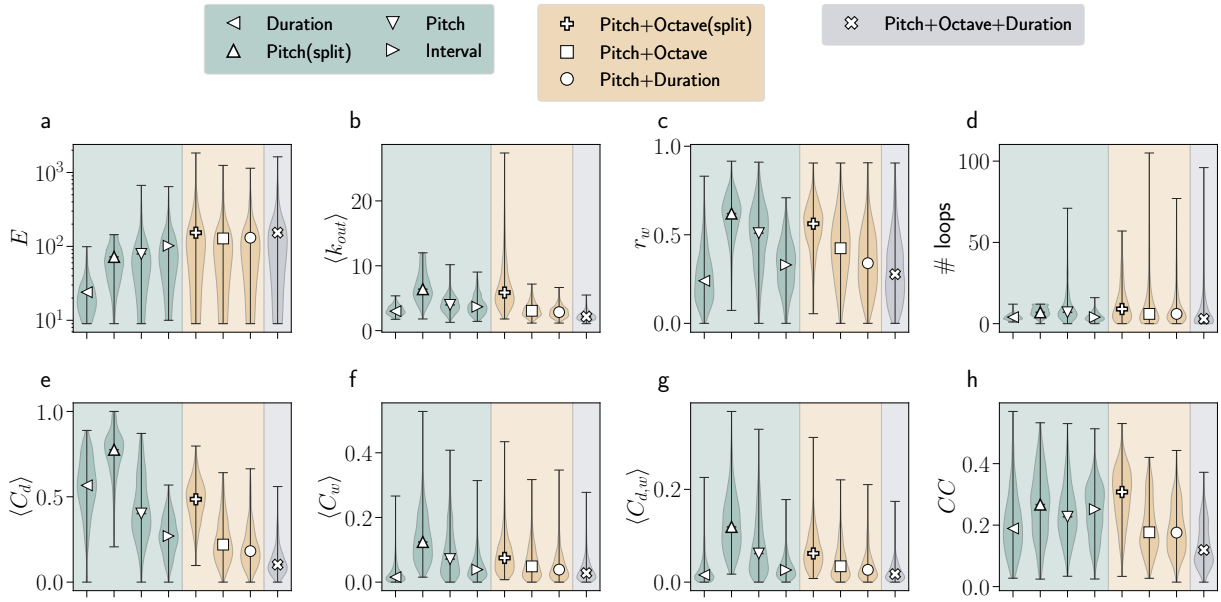


FIG. S4: Violin plots showing the distribution of eight network measures— (a) number of edges E , (b) average out-degree $\langle k_{out} \rangle$, (c) weighted reciprocity r_w , (d) number of self-loops $\# \text{ loops}$, (e) average directed and weighted clustering coefficient $\langle C_d \rangle$, (f) average undirected and weighted clustering coefficient $\langle C_w \rangle$, (g) average directed and weighted clustering coefficient $\langle C_{d,w} \rangle$, and (h) closeness centrality CC —across different models averaged over all music pieces for the **left** hand. Models are grouped by the number of musical features used. Each symbol corresponds to an individual model and also highlights the median of each distribution.

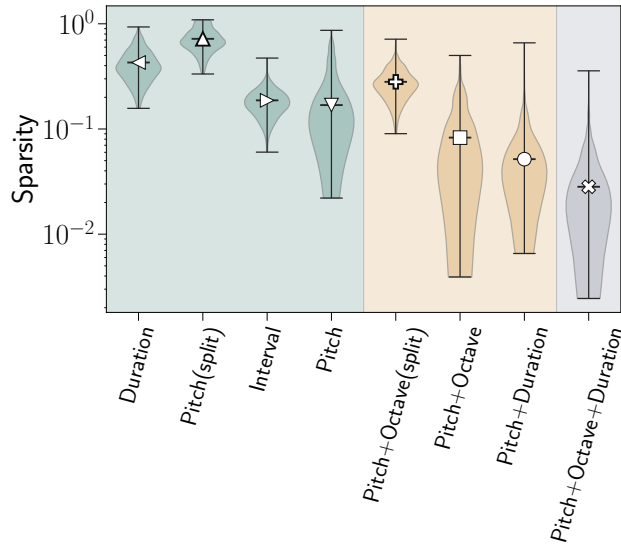


FIG. S5: Violin plots showing the distribution of sparsity across different models averaged over all music pieces for the **right** hand. Models are grouped by the number of musical features used. Each symbol corresponds to an individual model and also highlights the median of each distribution.

III. INFORMATION CONTENT AND PERCEPTION EFFICIENCY IN MUSIC NETWORKS

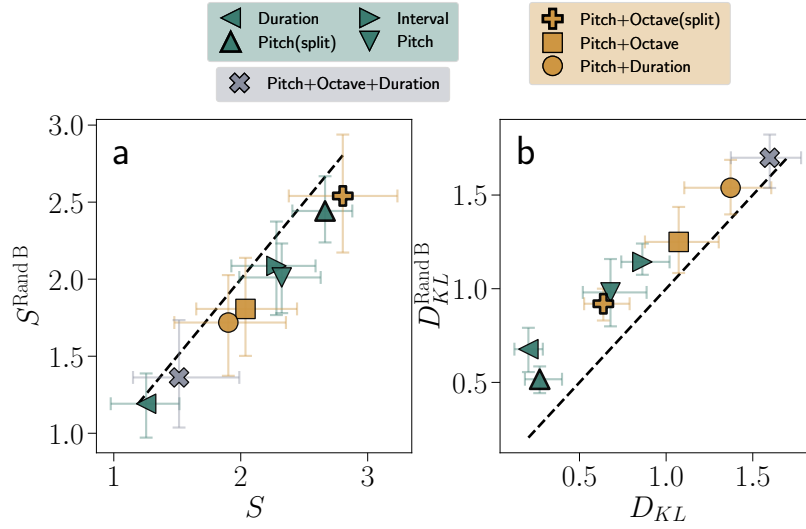


FIG. S6: **Information content and perception efficiency in music network models.** (a) Median entropy S versus entropy of type-B randomized networks. (b) Median D_{KL} versus D_{KL} of type-B randomized networks. Models are grouped by the number of musical features used. Each symbol corresponds to an individual model. Error bars show the interquartile range (IQR) around the median. All values correspond to right-hand tracks.

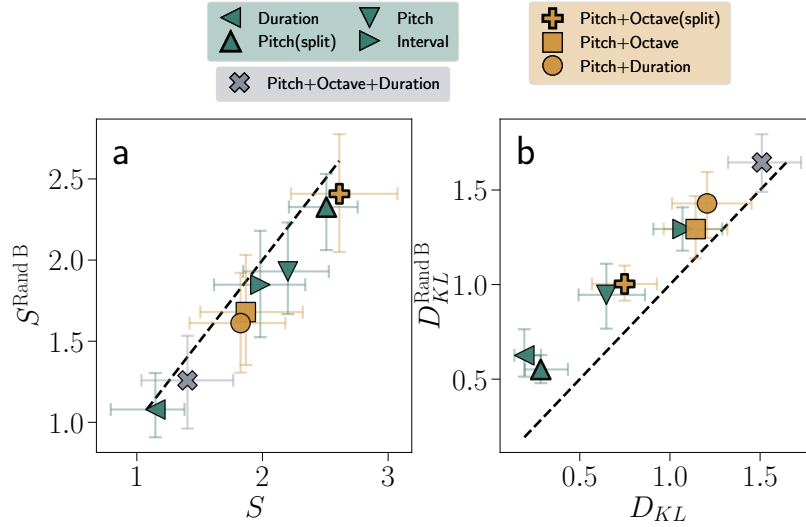


FIG. S7: **Information content and perception efficiency in music network models.** (a) Median entropy S versus entropy of type-B randomized networks. (b) Median D_{KL} versus D_{KL} of type-B randomized networks. Models are grouped by the number of musical features used. Each symbol corresponds to an individual model. Error bars show the interquartile range (IQR) around the median. All values correspond to left-hand tracks.

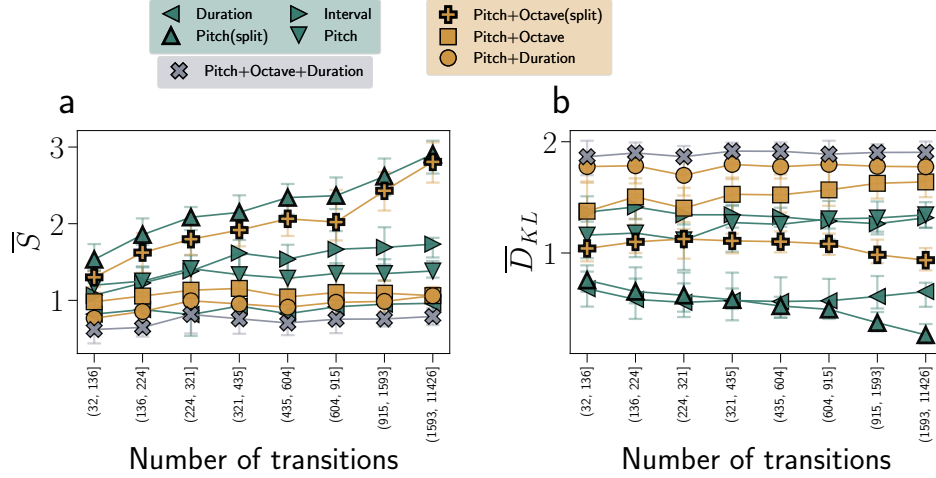


FIG. S8: (a) Median node-level entropy \bar{S} as a function of transition count. (b) Median node-averaged KL divergence \bar{D}_{KL} as a function of transition count. Transition counts are divided into eight equal-sized bins. Points show medians, and error bars indicate the interquartile range. All panels correspond to right-hand tracks.

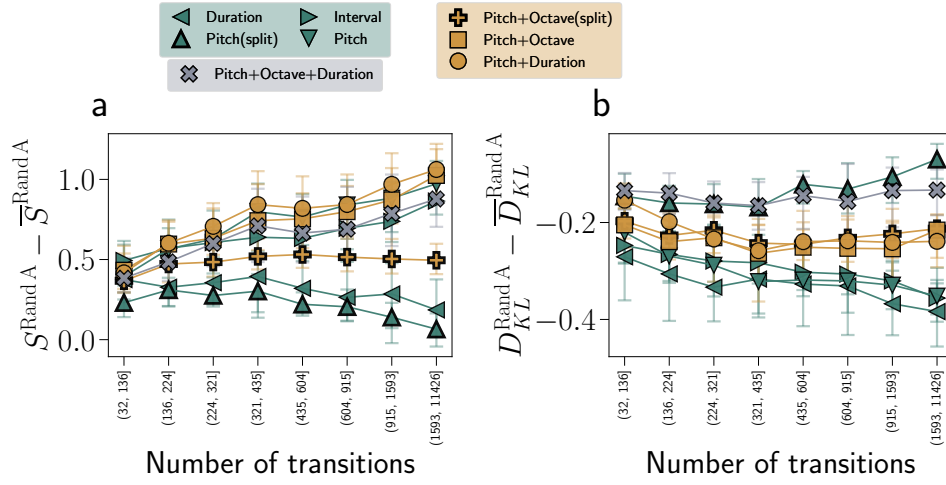


FIG. S9: (a) The difference between median entropy S and median node-level entropy \bar{S} of type-A randomized networks as a function of transition count. (b) The difference between median KL divergence D_{KL} and median node-averaged KL divergence \bar{D}_{KL} of type-A randomized networks as a function of transition count. Transition counts are divided into eight equal-sized bins. Points show medians, and error bars indicate the interquartile range. All panels correspond to right-hand tracks.

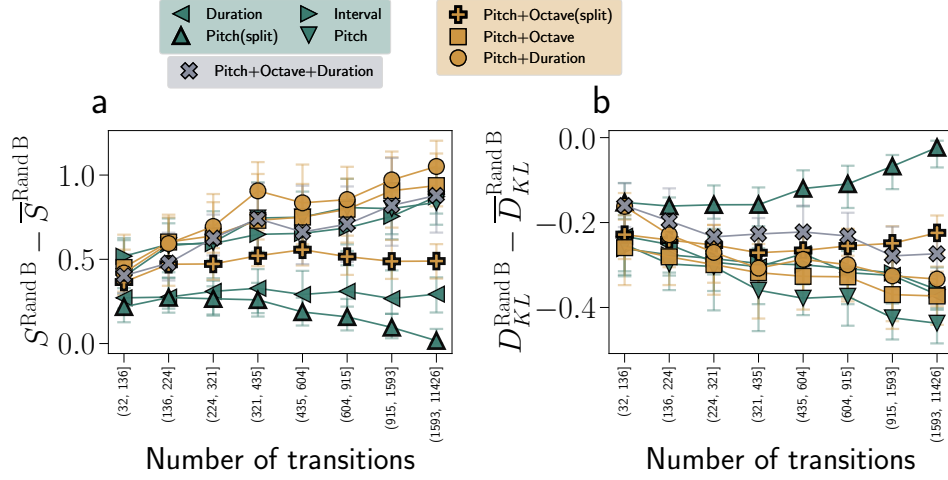


FIG. S10: (a) The difference between median entropy S and median node-level entropy \bar{S} of type-B randomized networks as a function of transition count. (b) The difference between median KL divergence D_{KL} and median node-averaged KL divergence \bar{D}_{KL} of type-B randomized networks as a function of transition count. Transition counts are divided into eight equal-sized bins. Points show medians, and error bars indicate the interquartile range. All panels correspond to right-hand tracks.

IV. DESCRIPTIVE ANALYSIS OF THE DATASETS

In Figure S11, we show the distribution of MIDI note numbers for both datasets. The left-hand notes range from 20 to 90, while the right-hand notes range from 40 to 110. In Figures S12-S13, we display the top 15 most frequent durations for the left and right hands. Generally, half and quarter notes occur very frequently, with whole notes following in the left hand and eighth notes in the right hand. These MIDI tracks are composed of sequences of notes that may be played simultaneously by one hand, forming chords. In Figure S14, we compared the number of pitches played by the left and right hands. In both datasets, the right hand predominantly plays single notes, while the left hand typically plays chords. Lastly, we looked at the most frequent chromatic intervals in both datasets. In Figures S15-S16, the left hand values exhibit a pronounced peak at interval 0, reflecting repeated pitches or unisons, whereas the right hand values show a dominant peak at -2, indicating a common descending two-semitones interval. Smaller secondary peaks highlight additional ascending and descending motions in both datasets.

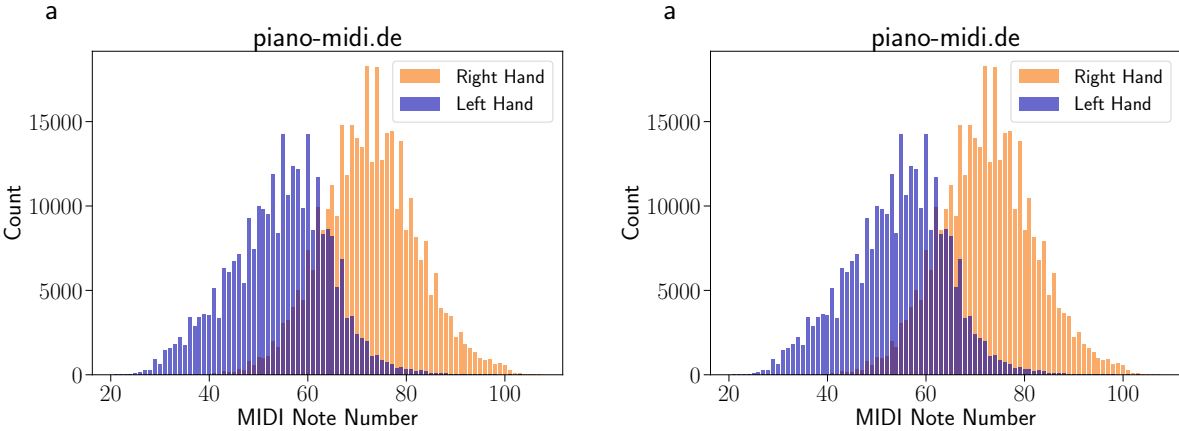


FIG. S11: The distribution of the MIDI note number for (a) piano-midi.de and (b) MSMD datasets.

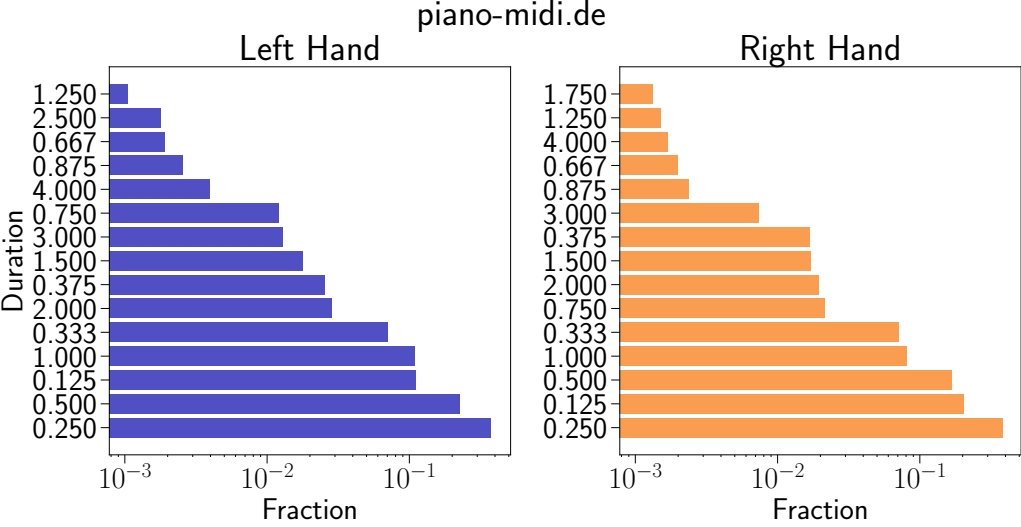


FIG. S12: Top 15 most frequent durations for the left and right hand parts from the piano-midi.de dataset.

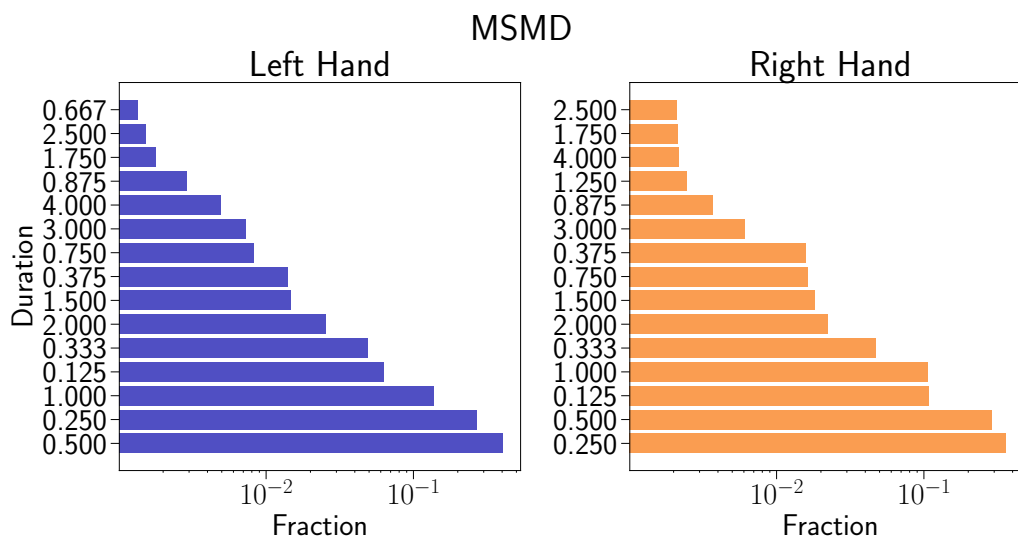


FIG. S13: Top 15 most frequent durations for the left and right hand parts from the MSMD dataset.

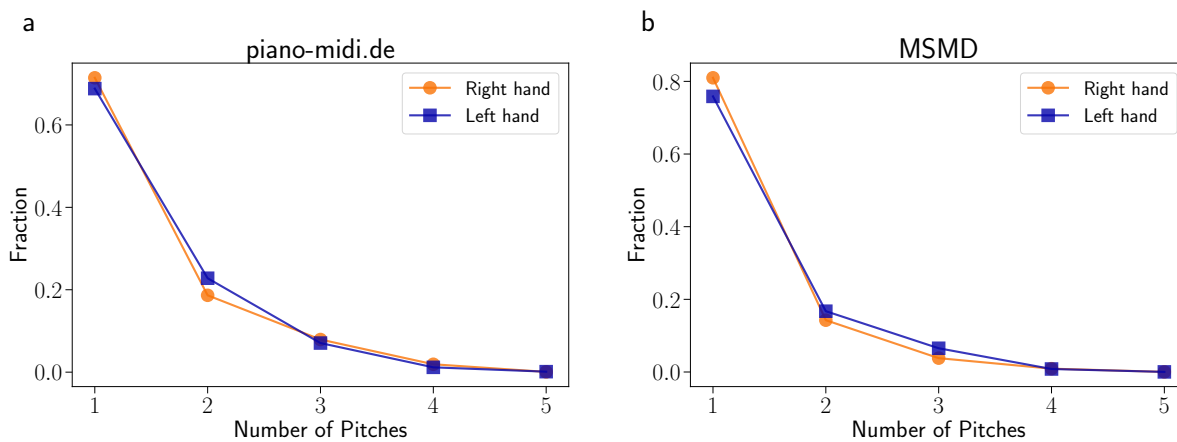


FIG. S14: Fraction of number of pitches for left and right hand for (a) piano-midi.de and (b) MSMD datasets.

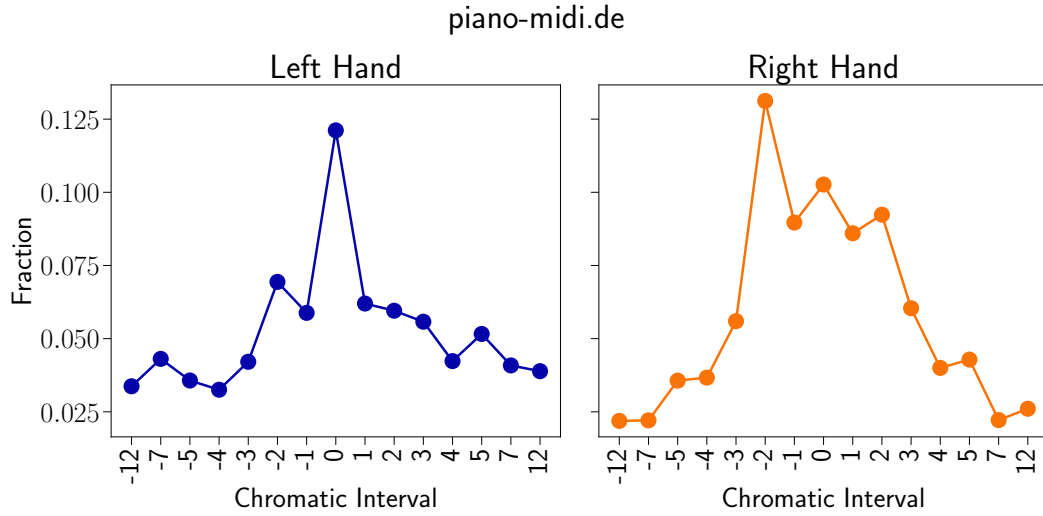


FIG. S15: Top 15 most frequent chromatic intervals for the left and right hand parts from the piano-midi.de dataset.

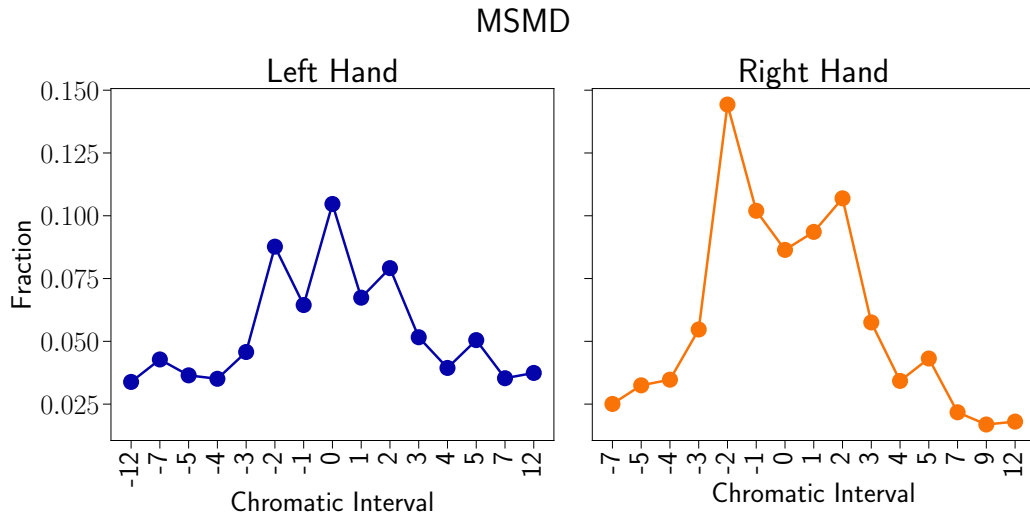


FIG. S16: Top 15 most frequent chromatic intervals for the left and right hand parts from the MSMD dataset.

